Highly Accurate *in Vivo* Terahertz Spectroscopy of Healthy Skin: Variation of Refractive Index and Absorption Coefficient Along the Human Body

Kirill I. Zaytsev, Arseniy A. Gavdush, Nikita V. Chernomyrdin, and Stanislav O. Yurchenko

***Abstract*—A method to reconstruct the terahertz (THz) refractive index and absorption coefficient of *in vivo* tissue using THz pulsed spectroscopy (TPS) has been proposed. The method utilizes a reference THz window to fix the sample of interest during the TPS reflection mode measurements. Satellite pulses caused by multiple THz-wave reflections in the reference window are taken into account to accurately solve the inverse problem. The stability of the proposed method in the presence of various factors, including digital noise in the TPS waveforms and fluctuations of the reference THz window position, has been accurately analyzed. The method has been implemented to study *in vivo* the THz refractive index and absorption coefficient of the human skin. The skin from three persons has been measured, and the results agree with the well-known data on healthy skin spectroscopy in general, except for several regions of the skin. Thus, for the elbow, the hand, the knee, and the heel the THz refractive index and absorption coefficient considerably differ from the average values. The observed results are of principle importance for further development of novel approaches to skin diagnosis based on THz technologies.**

***Index Terms*—Absorption coefficient, inverse problem, material parameters, refractive index, spectroscopy of the skin, terahertz pulsed spectroscopy, THz technology.**

I. Introduction

TERAHERTZ (THz) pulsed spectroscopy (TPS) recently has attracted considerable interest as a prospective method of medical diagnosis [1]–[5].

TPS first appeared as a result of Auston's research on semiconductor photoconductivity [6], [7]. It was rapidly developed through novel techniques to generate and detect THz pulses [8]–[20]. Methods of characterizing the THz material parameters [21]–[31], as well as methods of THz time-of-flight tomography [32]–[35], have been proposed. Its applicability to noninvasive medical diagnosis of oral, [36] skin, [37]–[40] colon [41], [42], and liver [43] cancers and to intraoperative diagnosis of breast cancer [44]–[47] has been considered. In [48], [49] it was shown, that the exposure of artificial human skin tissue to the intense picosecond THz pulses affects the expression levels of genes, associated with non-melanoma cancers and inflammatory diseases of the skin. The ability to cause favorable changes in the expression of genes indicates prospectives of therapeutic applications of THz radiation. The use of TPS for sensing in corneal tissue [50], dental tissue [51], [52], and blood [53]–[55], as well as for studying thermal and chemical tissue burns [56]–[59], has been studied. In [60] and [61], the ability to noninvasively diagnose dysplastic skin nevi has been demonstrated; this is of importance since the dysplasia of skin nevi is considered to be a melanoma precursor, which is reportedly the most dangerous skin cancer [62], [63]. Despite the wide variety of biomedical applications of TPS, the development of novel methods for TPS signal processing and the inverse problem solution is of great importance for further progress of TPS technology.

In this paper, we describe a method to reconstruct the THz refractive index and absorption coefficient of *in vivo* tissue based on TPS signal processing. The method implies reflection mode measurement of the sample, while it is placed behind a reference SiO_2-window. We take into account satellite pulses, appearing as a result of the multiple THz-wave reflections in the reference window, thereby allowing us to significantly increase the accuracy of the inverse problem solution. The stability of the proposed method in the presence of various factors, including TPS waveform noise and fluctuations of the reference window position, is studied by means of numerical modeling. We implement the method to study *in vivo* the THz refractive index and absorption coefficient of the skin from three persons. Observed results agree with the well-known data in general. However, we demonstrate significant fluctuations of THz characteristics of the skin along the various skin regions, in particular, the hand, the knee, and the heel. These fluctuations should be taken into account for further development of novel methods of skin diagnosis using TPS.

This paper is organized as follows. In Section II, we briefly discuss the TPS setup utilized to study the skin. In Section III, we introduce the method to reconstruct the THz refractive index and absorption coefficient of tissue *in vivo*. Section III-A introduces an approach both for studying the stability of the inverse problem solution and for estimating the reconstruction error

Manuscript received March 28, 2015; revised May 16, 2015; accepted July 21, 2015. Date of publication August 24, 2015; date of current version August 31, 2015. The work of A. A. Gavdush and N. V. Chernomyrdin was supported by the Russian Foundation for Basic Research under Projects 14-02-00781, 14-08-31124, 14-08-31102, and 15-32-20575. The work of K. I. Zaytsev and S. O. Yourchenko was supported by the Government of the Russian Federation under Grant 074-U01. *(Corresponding authors: Kirill I. Zaytsev and Stanislav O. Yurchenko.)*

K. I. Zaytsev and N. V. Chernomyrdin are with Bauman Moscow State Technical University, 105005, Moscow, Russia, with ITMO University, 197101, Saint-Petersburg, Russia, and also with I. M. Sechenov First Moscow State Medical University, 119048, Moscow, Russia (e-mail: kirzay@gmail.com).

A. A. Gavdush and S. O. Yourchenko are with the Bauman Moscow State Technical University, 105005, Moscow, Russia, and also with the ITMO University, 197101, Saint-Petersburg, Russia (e-mail: st.yurchenko@mail.ru).

Color versions of one or more of the figures in this paper are available online at http://ieeexplore.ieee.org.

Digital Object Identifier 10.1109/TTHZ.2015.2460677

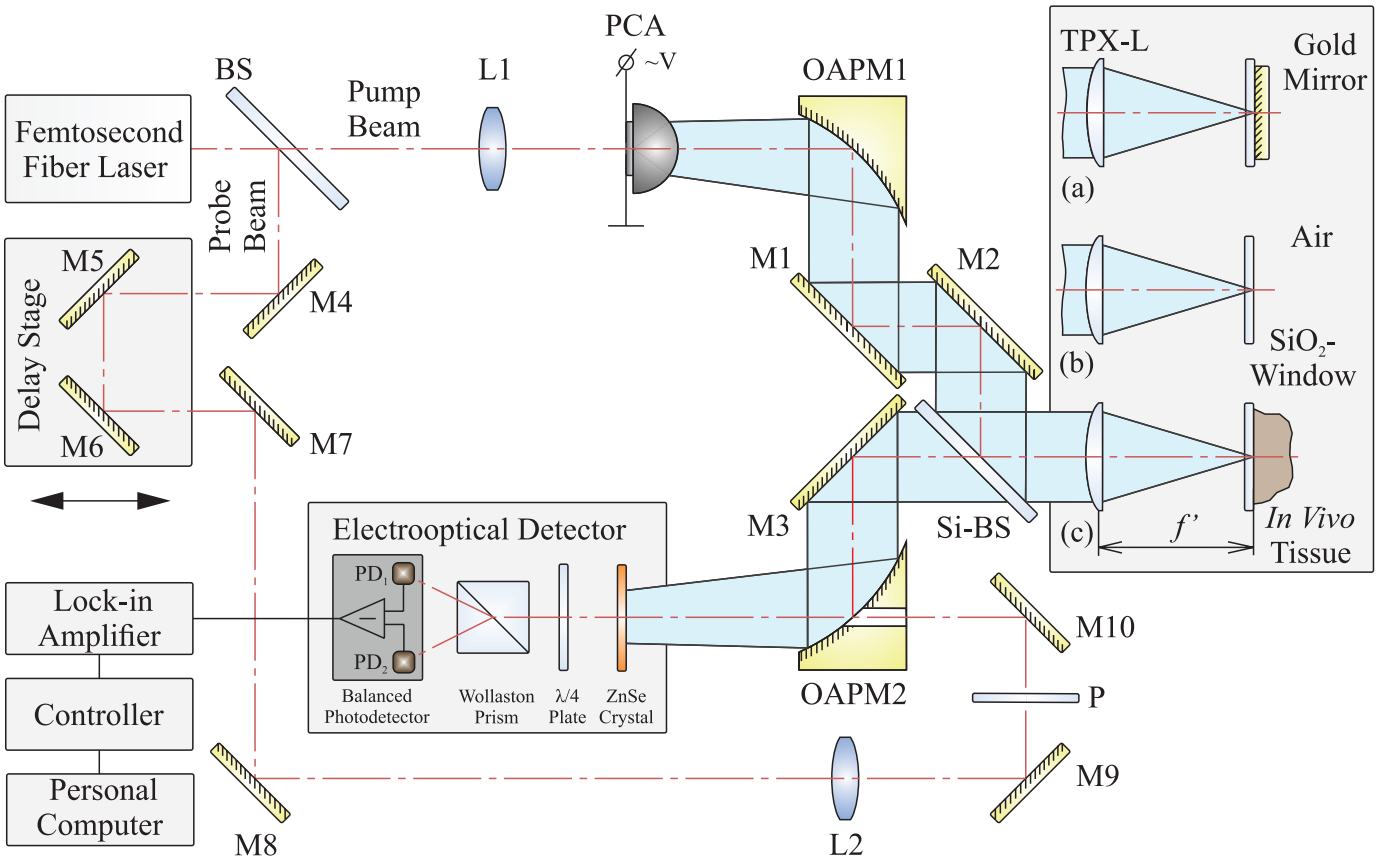

Fig. 1. Schematic representation of experimental setup: BS and Si-BS stand for beamsplitters operating in the optical and the THz ranges, respectively, PCA stands for the LT-GaAs-photoconductive antenna, L1 and L2 stand for optical lenses, TPX-L stands for the THz lens made of polymethylpentene, M1–M10 stand for plane gold-coated mirrors, OAPM1 and OAPM2 stand for off-axial gold-coated parabolic mirrors, and P stands for the optical polarizer. Panels (a), (b), and (c) illustrate the process of TPS waveform detection: (a) corresponds to the waveform E_m reflected from the window with the gold mirror behind; (b) corresponds to the waveform E_r, reflected from the empty window; (c) corresponds to the sample waveform E_s.

based on numerical simulations. In Section III-B and III-C, we examine the instability of the inverse problem solution in the presence of digital noises in the TPS waveforms and fluctuations of the reference window position, respectively. In Section III-D we verify the proposed method by comparing our results on healthy skin characterization *in vivo* with the well-known data. Section IV presents the results of systematic *in vivo* THz spectroscopy of various skin regions. Section V summarizes the results of the paper.

II. Experimental Setup

In the present work we use a compact TPS setup, which is similar to the one described in [35]. The setup operates in reflection mode and allows us to measure the THz spectra between 0.1 and 2.5 THz.

Fig. 1 schematically represents the experimental setup and illustrates the process of TPS waveform detection. The TPS system utilizes the second-harmonic radiation of the Er-doped femtosecond fiber laser with an average power of 200 mW for both THz pulse generation and detection. The central wavelength is 780 nm, and the pulse duration and the pulsed repetition rate are 100 fs and 60 MHz, respectively. THz-wave generation is produced in a LT-GaAs-photoconductive antenna [10], and detection of THz pulses is conducted in a ZnTe-electro-optical detector [14].

We perform the reflection mode measurements with a beamsplitter and a normal angle of radiation incidence on the sample surface. The sample waveform is obtained while sample is placed behind the reference 1-mm-thick window made of crystalline quartz. The window allows us to fix the sample toward the TPS setup. Thus, the interface between the SiO_2 and the sample is located at the TPX-lens focus [Fig. 1(c)].

III. Reconstruction of THz Refractive Index and Absorption Coefficient

Three THz waveforms are detected to characterize a single sample: the waveform $E_m = E_m(t)$ reflected from the reference window with a gold mirror placed behind [Fig. 1(a)], the waveform $E_r = E_r(t)$ reflected from the empty reference window [Fig. 1(b)], and the waveform $E_s = E_s(t)$ reflected from the reference window with the sample of interest placed behind [Fig. 1(c)]. Let us define the Fourier spectrums of E_m, E_r, and E_s as $\widetilde{E}_m = \widetilde{E}_m(\nu)$, $\widetilde{E}_r = \widetilde{E}_r(\nu)$, and $\widetilde{E}_s = \widetilde{E}_s(\nu)$, where ν is an electromagnetic wave frequency.

Fig. 2 shows the typical waveforms observed during *in vivo* spectroscopy of the skin: (a), (b) and (c) correspond to E_m, E_r and E_s. The waveforms contain the first pulse, reflected from the interface between air and the reference window (region (I) in Fig. 2), the second pulse, reflected from the interface between the reference window and the mirror, the reference window and the air, or the reference window and the sample (region (II)

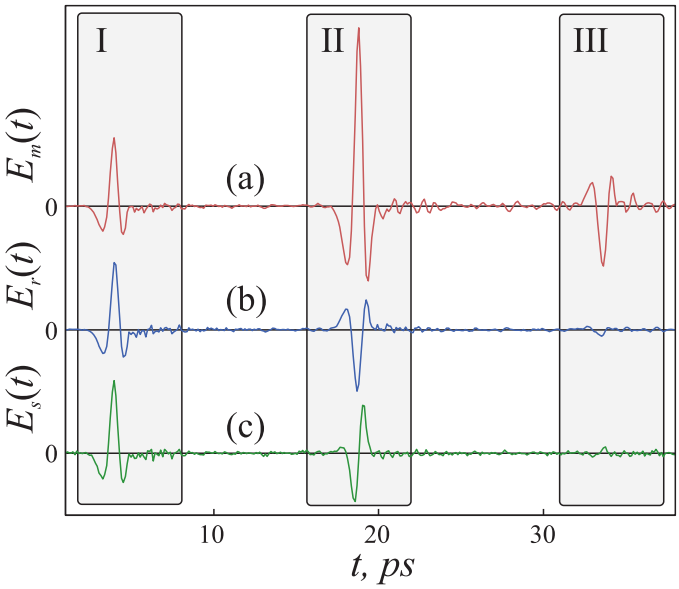

Fig. 2. TPS waveforms corresponding to the THz pulse reflection (a) from the reference window with the gold mirror placed behind E_m, (b) from the empty reference window E_r, and (c) from the reference window with the sample of interest placed behind E_s. Regions (I), (II), and (III) in all the waveforms indicate the reference, the sample, and the first satellite pulses, respectively.

in Fig. 2), and the third pulse (the first satellite pulse), originating owing to the multiple THz-wave reflections in the reference window (region (III) in Fig. 2). The first pulse remains the same for all the waveforms, since it reflects from the front surface of the reference window. Therefore, we use it to estimate the uniform zero point of the signals in the time-domain. The second pulse and the first satellite pulse are taken into account to reconstruct the THz refractive index and absorption coefficient of the sample. We will show below that consideration of the satellite pulses allows us to significantly raise the reconstruction accuracy.

Our method allows reconstruction of the THz refractive index $n = n(\nu)$ and absorption coefficient $\alpha = \alpha(\nu)$ of the sample, which are related to the complex sample refractive index $\widetilde{n} = \widetilde{n}(\nu)$

$$\widetilde{n} = n - i\frac{c}{2\pi\nu}\alpha \tag{1}$$

where $c \simeq 3 \times 10^8$ m/s stands for the speed of light in vacuum. We reconstruct the complex refractive index of the sample, and the solution of this inverse problem should minimize an error functional

$$\widetilde{n} = \arg\min_{\widetilde{n}}[\Phi] \tag{2}$$

where

$$\Phi = \left|\left|\widetilde{H}_{exp}\right| - \left|\widetilde{H}_{th}\right|\right|^2 + \left|\phi\left[\widetilde{H}_{exp}\right] - \phi\left[\widetilde{H}_{th}\right]\right|^2 \tag{3}$$

where $\widetilde{H}_{exp} = \widetilde{H}_{exp}(\nu)$ and $\widetilde{H}_{th} = \widetilde{H}_{th}(\nu, \widetilde{n})$ are experimental and theoretical transfer functions, $|\ldots|$ and $\phi[\ldots]$ are operators to extract the modulus and the phase.

We define the experimental transfer function as

$$\widetilde{H}_{exp} = \frac{\widetilde{E}_s - \widetilde{E}_r}{\widetilde{E}_m - \widetilde{E}_r}. \tag{4}$$

For the theoretical transfer function we assume satellite pulses originating from the multiple THz-wave reflections in the reference window:

$$\widetilde{H}_{th} = \frac{\widetilde{R}_{12} - \widetilde{R}_{10} + \sum_{j=1}^{N}(\widetilde{R}_{12}^{j+1} - \widetilde{R}_{10}^{j+1})\widetilde{R}_{10}^{j}\widetilde{P}_1^{2j}}{\widetilde{R}_{13} - \widetilde{R}_{10} + \sum_{j=1}^{N}(\widetilde{R}_{13}^{j+1} - \widetilde{R}_{10}^{j+1})\widetilde{R}_{10}^{j}\widetilde{P}_1^{2j}} \tag{5}$$

where $\widetilde{R}_{mk} = \widetilde{R}_{mk}(\nu, \widetilde{n}_m, \widetilde{n}_k)$ describes the Fresnel reflection at the interface of mth and kth media:

$$\widetilde{R}_{mk} = \frac{\widetilde{n}_k - \widetilde{n}_m}{\widetilde{n}_m + \widetilde{n}_k}. \tag{6}$$

The indices $m, k = 0, 1, 2,$ and 3 correspond to the air, SiO_2, tissue, and gold mirror media, respectively. $\widetilde{P}_1 = \widetilde{P}_1(\nu, \widetilde{n}_1, l)$ is based on the Bouguer–Lambert–Beer law describing the THz-wave propagation along a distance l in the reference SiO_2 window

$$\widetilde{P}_1 = \exp\left(-i\frac{2\pi\nu}{c}\widetilde{n}_1 l\right). \tag{7}$$

In (5)–(7), the complex refractive indices of air and SiO_2 ($\widetilde{n}_0$ and $\widetilde{n}_1$), the effective complex refractive index of the gold mirror ($\widetilde{n}_3$), the number of satellite pulses (N), and the thickness of the reference window (l) are known *a priori*, and the THz complex refractive index of the sample ($\widetilde{n} = \widetilde{n}_2$) is estimated via (2).

In contrast to the well-known methods used to determine the THz material parameters via the reflection-mode measurements (for instance, see [24]), in the described approach we assume multiple THz-wave reflections in the reference window, thereby allowing us to significantly increase the reconstruction accuracy. To examine the impact of the sample transfer function determination error $\Delta\widetilde{H}_{th}$ on the reconstruction error $\Delta\widetilde{n}$ for various numbers of satellite pulses N, we implement the local linearization [28], [64] of the theoretical transfer function (5)

$$\Delta\widetilde{n} = \widetilde{K}\Delta\widetilde{H}_{\rm th} \tag{8}$$

where $\widetilde{K} = \widetilde{K}(N, \nu, \widetilde{n}_1, \widetilde{n}, l)$ is a complex coefficient of the local linearization. By calculating $\widetilde{K}$ for typical experimental conditions (for simplicity, we assume, that $n_1 = 2.14$ and $\alpha_1 = 0$ are the THz refractive index and absorption coefficient of the reference window at $\nu = 1.0$ THz, $l = 1.0$ mm is the thickness of this window, and $n = 1.57$ and $\alpha = 13$ mm^{-1} are the typical values of THz refractive index and absorption coefficient of the skin tissue *in vivo* at $\nu = 1.0$ THz), we determine the dependence $\widetilde{K}(N)$, which is presented in Fig. 3 as the modulus $|\widetilde{K}|$ and the phase $\phi[\widetilde{K}]$.

One can observe that $|\widetilde{K}|$ decreases with an increase of N. Thus, the more satellite pulses are considered, the higher the reconstruction accuracy is. Moreover, $\phi(\widetilde{K})$ significantly varies with N; therefore, the impact of $\Delta\widetilde{H}_{th}$ on reconstruction of the real and imaginary parts of the complex refractive index and, as a consequence, on reconstruction of the THz refractive

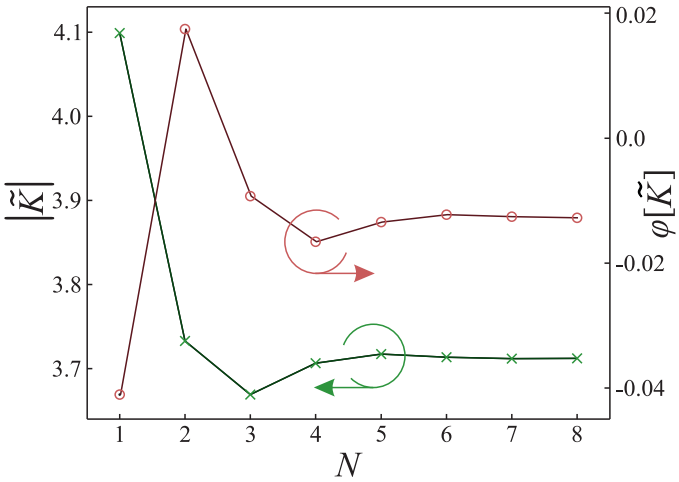

Fig. 3. The modulus $|\widetilde{K}|$ and the phase $\phi[\widetilde{K}]$ of the local linearization coefficients $\widetilde{K}(N)$ (8) calculated for the typical conditions of the experiment: $n_1 = 2.14$ and $\alpha_1 = 0$ are the THz refractive index and absorption coefficient of the reference window at $\nu = 1.0$ THz, $l = 1.0$ mm is the thickness of this reference window, and $n = 1.57$ and $\alpha = 13$ mm^{-1} are the typical THz refractive index and absorption coefficient of the skin tissue *in vivo* at $\nu = 1.0$ THz.

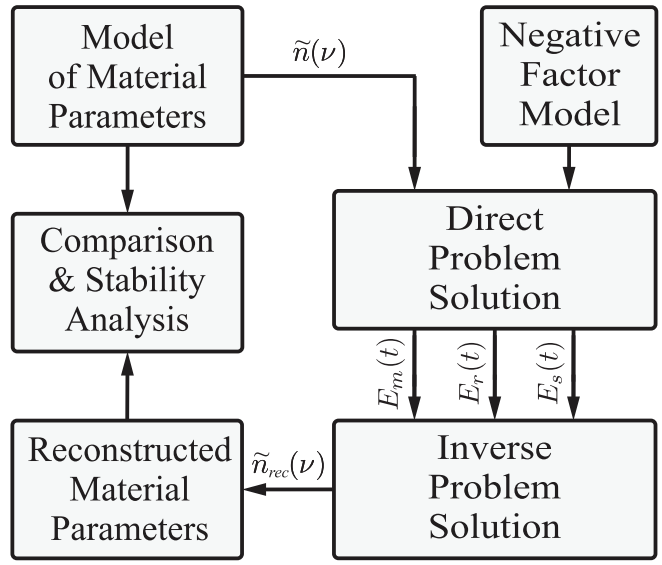

Fig. 4. Schematic representation of the method applied to examining the stability of THz refractive index and absorption coefficient reconstruction.

index and absorption coefficient differs for various N. For specified local linearization conditions the accuracy of reconstruction could be 10% higher in case of even one satellite pulse is taken into account.

Many factors affect the process of THz refractive index and absorption coefficient reconstruction. The list of factors, which are inherent specifically to the proposed method, includes digital noise in the TPS waveforms, spectral inhomogeneity of the TPS sensitivity, and fluctuations of the reference window position, caused by movements of the sample *in vivo*. All these factors should be considered during solution of the inverse problem and estimation of the reconstruction error [28], [65].

A. Numerical Approach to Examine the Stability of the Inverse Problem Solution

We study the stability of the inverse problem solution by means of numerical simulations of the algorithm implementation in the presence of specified negative factors (see Fig. 4).

First, we define the model of THz material parameters of the sample. We use the well-known model of the THz material parameters of the skin $\widetilde{n} = \widetilde{n}(\nu)$, which are described with the double-Debye model [66]

$$\widetilde{n} = \sqrt{\widetilde{\varepsilon}}, \quad \widetilde{\varepsilon} = \varepsilon_\infty + \frac{\varepsilon_s - \varepsilon_2}{1 + i2\pi\nu\tau_1} + \frac{\varepsilon_2 - \varepsilon_\infty}{1 + i2\pi\nu\tau_2} \tag{9}$$

where $\widetilde{\varepsilon} = \widetilde{\varepsilon}(\nu)$ is a complex dielectric permittivity, ε_s, ε_2, and ε_∞ are dielectric parameters, τ_1 and τ_2 are relaxation times in the medium (Table I).

Second, we solve the direct problem. A Gaussian monopulse function $E_0 = E_0(t)$ [35] is assumed to describe the THz-pulse radiating the sample

$$E_0 = -2e^{1/2}(\pi\nu_c t)\exp(-2(\pi\nu_c t)^2) \tag{10}$$

where $\nu_c = 0.95$ THz stands for a central frequency of the Gaussian monopulse. The Fourier spectrums of the waveforms $\widetilde{E}_m$, $\widetilde{E}_r$ and $\widetilde{E}_s$, which form the basis for the inverse problem

TABLE I
DOUBLE-DEBYE MODEL PARAMETERS FOR THE THZ COMPLEX DIELECTRIC PERMITTIVITY OF THE SKIN *IN* VIVO [66]

ε_s	ε_2	ε_∞	τ_1 (ps)	τ_2 (ps)
60.0	3.6	3.0	10.0	0.2

solution, are modeled based on the Fresnel formulas (6) and the Beer–Lambert–Bouger law (7)

$$\begin{aligned}
\widetilde{E}_m &= \widetilde{E}_0\left(R_{01} + T_{01}T_{10}P_1^2\left(R_{13} + \sum_{j=1}^{N} P_1^{2j}R_{13}^{j+1}R_{10}^{j}\right)\right)\\
\widetilde{E}_r &= \widetilde{E}_0\left(R_{01} + T_{01}T_{10}P_1^2\left(R_{10} + \sum_{j=1}^{N} P_1^{2j}R_{10}^{2j+1}\right)\right)\\
\widetilde{E}_s &= \widetilde{E}_0\left(R_{01} + T_{01}T_{10}P_1^2\left(R_{12} + \sum_{j=1}^{N} P_1^{2j}R_{12}^{j+1}R_{10}^{j}\right)\right)
\end{aligned} \tag{11}$$

where $\widetilde{E}_0 = \widetilde{E}_0(\nu)$ stands for the Fourier spectrum of the Gaussian monopulse (10) describing the spectral inhomogeneity of the TPS sensitivity; indices 0, 1, 2, and 3 correspond to the air, SiO_2, tissue, and gold media, respectively. In (11) one satellite pulse is considered, i.e., $N = 1$. The thickness of the reference window is $l = 1$ mm, and the THz material parameters of the reference window represent the crystalline quartz [67]. A time-domain representation of the waveforms is obtained via the inverse Fourier transform

$$E_m = \mathcal{F}_\nu^{-1}[\widetilde{E}_m], \quad E_r = \mathcal{F}_\nu^{-1}\left[\widetilde{E}_r\right], \quad E_s = \mathcal{F}_\nu^{-1}\left[\widetilde{E}_s\right] \tag{12}$$

where $\mathcal{F}_\nu^{-1}$ stands for the inverse Fourier transform operator. Equations (10)–(12) allow us to solve the direct problem, namely, to simulate the backscattering of the THz pulse and to estimate the waveforms.

Finally, the inverse problem is solved via (2), which results in the reconstructed material parameters $\widetilde{n}_{\rm rec} = \widetilde{n}_{\rm rec}(\nu)$. To study the stability of the inverse problem solution, we introduce the negative factors of reconstruction (digital noise in the TPS waveforms and translational and angular fluctuations of the reference window position) at the stage of the direct problem solution [see (10)–(12)], and then obtain the distorted TPS waveforms and solve the inverse problem (2). The errors of the THz refractive index and absorption coefficient reconstruction are calculated via a comparison of the initial, $\widetilde{n}$, and the reconstructed, $\widetilde{n}_{\rm rec}$, parameters.

Notice, the described approach (Fig. 4) also allows us to examine the experimental error of the THz material parameter reconstruction, namely, to calculate the error bars.

B. Digital Noise in the TPS Waveforms

Let us consider the inverse problem instability caused by digital noise in the TPS waveforms. We assume white Gaussian noise distorting the waveforms in (12)

$$E'_m = E_m + \varsigma_m, \quad E'_r = E_r + \varsigma_r, \quad E'_s = E_s + \varsigma_s \qquad (13)$$

where $\varsigma_m = \varsigma_m(t, \sigma_N)$, $\varsigma_r = \varsigma_r(t, \sigma_N)$ and $\varsigma_s = \varsigma_s(t, \sigma_N)$ correspond to different realizations of Gaussian noise with uniform standard deviation σ_N. The noise is introduced in the time-domain [68], and σ_N is defined in fractions of the maximal amplitude of the reference THz pulse (region (I) in the Fig. 2).

We perform a set of equal numerical experiments with different noise realizations, $\varsigma_{m,p}$, $\varsigma_{r,p}$ and $\varsigma_{s,p}$. This leads to the set of reconstruction results $\widetilde{n}_{rec,p}$, where $p = 1, 2, \ldots, M$ is the experiment number. By comparing $\widetilde{n} = n - i\alpha c/(2\pi\nu)$ and $\widetilde{n}_{rec,p} = n_{rec,p} - i\alpha_{rec,p}c/(2\pi\nu)$, we calculate the normalized spectral densities of the reconstruction errors

$$\frac{\Delta n}{n} = \frac{1}{n}\sqrt{\frac{1}{M}\sum_{p=1}^{M}|n_{rec,p} - n|^2},$$
$$\frac{\Delta \alpha}{\alpha} = \frac{1}{\alpha}\sqrt{\frac{1}{M}\sum_{p=1}^{M}|\alpha_{rec,p} - \alpha|^2} \qquad (14)$$

where $M \to +\infty$ is the number of numerical experiments. Fig. 5 shows the results of these calculations: (a) shows the initial model of the THz refractive index and absorption coefficient, n and α, as well as the results of the inverse problem solution, $n_{rec,p}$ and $\alpha_{rec,p}$, calculated for $\sigma_N = 0.3\%$; (b) and (c) shows the normalized spectral densities of the errors of the refractive index and the absorption coefficient reconstruction, $\Delta n/n$ and $\Delta\alpha/\alpha$.

The noise leads to significant distortions in the reconstruction results. The observed errors have stochastic character, and the error magnitude varies inhomogeneously with frequency [Fig. 5(a)]. The standard deviation $\sigma_N \leq 0.2\%$ allows accurate reconstruction of the THz material parameters in a reliable frequency range of 0.2 to 1.4 THz [Fig. 5(b) and 5(c)]. This standard deviation can be easily achieved via the waveform averaging or by implementing the effective methods of TPS waveform denoising [69]–[71].

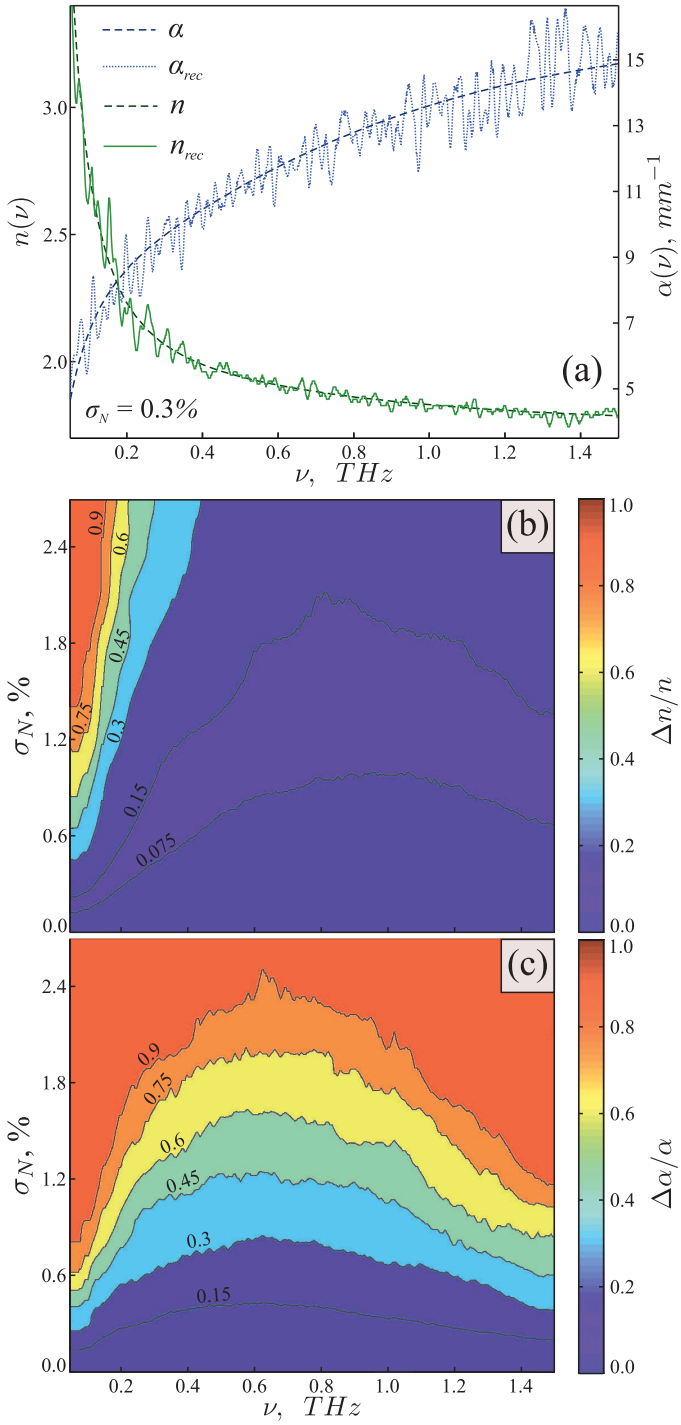

Fig. 5. Impact of white Gaussian noise in the TPS waveforms (13) on the reconstruction of the THz refractive index and absorption coefficient of the skin *in vivo*. (a) Initial model of THz refractive index and absorption coefficient, n and α, and the reconstructed curves, $n_{{\rm rec},p}$ and $\alpha_{{\rm rec},p}$, calculated for $\sigma_N = 0.3\%$. (b) Normalized spectral density of the refractive index reconstruction error $\Delta n/n$ (14). (c) Normalized spectral density of the absorption coefficient reconstruction error $\Delta\alpha/\alpha$ (14).

C. Fluctuations of the Reference Window Position

The person (patient) can easily impact the reference window position by pressing it during the sample waveform detection. This may cause errors in the inverse problem solution. Reference window fluctuations can be divided into two types: 1) the

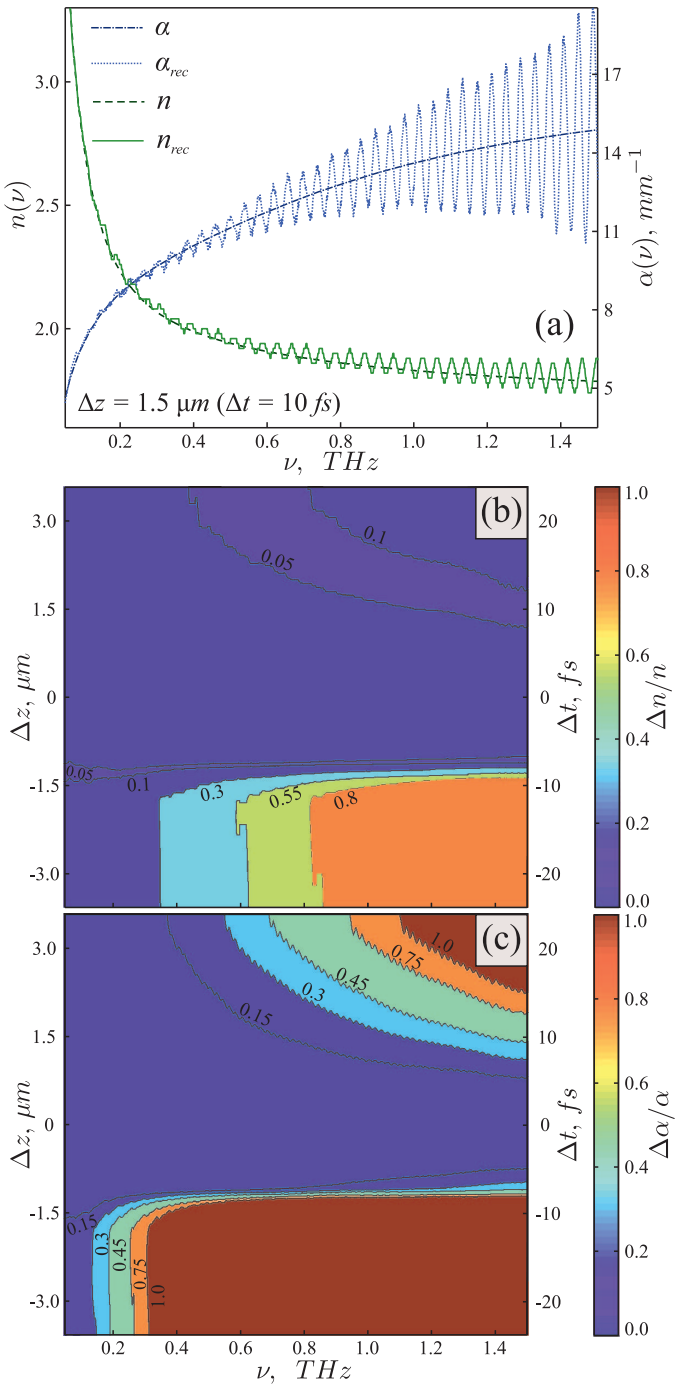

Fig. 6. Impact of the reference window translation (15) on reconstruction of the THz refractive index and absorption coefficient of the skin *in vivo*. (a) Initial model of the THz refractive index and absorption coefficient, n and α, and the reconstructed curves, $n_{\rm rec}$ and $\alpha_{\rm rec}$, calculated for $\Delta z = +1.5$ μm ($\Delta t = +10$ fs). (b) Normalized spectral density of the refractive index reconstruction error $\Delta n/n$ (16). (c) Normalized spectral density of the absorption coefficient reconstruction error $\Delta\alpha/\alpha$ (16).

linear translation along the THz beam axis and 2) the deviation of the angular orientation (Fig. 1).

For Δz linear translation of the reference window in the direction of the TPS lens (positive direction), we observe Δt translation of the sample waveform

$$E_s' = E_s(t+\Delta t), \quad \Delta t = 2\frac{\Delta z}{c}. \tag{15}$$

This time-domain translation leads to the appearance of the reconstruction errors. We apply numerical simulations to solve the direct and the inverse problems in the presence of this factor for various Δt, and Fig. 6 shows the results.

Fig. 6(a) illustrates the typical character of the noise in reconstructed THz refractive index and absorption coefficient owing to $\Delta z = +1.5$ μm ($\Delta t = +10$ fs). The noise in $n_{\rm rec}$ and $\alpha_{\rm rec}$ exhibit an oscillating character, and its magnitude varies inhomogeneously with frequency. Fig. 6(b) and 6(c) shows the normalized spectral densities of the noise magnitude, $\Delta n/n$ and $\Delta\alpha/\alpha$, caused by various Δt. Notice that $\Delta n/n$ and $\Delta\alpha/\alpha$ are estimated via the grayscale morphological closing [72]

$$\frac{\Delta n}{n} = \frac{1}{n}\Big(\big((n_{rec,p}-n)\oplus a\big)\ominus a\Big)$$
$$\frac{\Delta \alpha}{\alpha} = \frac{1}{\alpha}\Big(\big((\alpha_{rec,p}-\alpha)\oplus a\big)\ominus a\Big) \tag{16}$$

where $(f\oplus a)$ stands for the grayscale delotation of f by the primitive of a size, $(f\ominus a)$ stands for the grayscale erosion of f by the primitive of a size, and a is chosen to be wider then the period of the error oscillations [Fig. 6(a)].

The functions $\Delta n/n$ and $\Delta\alpha/\alpha$ have asymmetric character with respect to the ideal position of the window $\Delta t = 0$ ($\Delta z = 0$). One can notice significant distortions caused by even small translations of the reference window, $|\Delta z| > 1.2$ μm($|\Delta t| > 8$ fs). Therefore, for the correct solution of the inverse problem we should apply TPS waveforms preprocessing in order to estimate the uniform zero point of waveforms E_m, E_r, and E_s in time-domain. In the present work we use the correlation procedure [72] to accurately solve this problem.

Another distortion of the reconstruction results is caused by the angular deviation of the reference window orientation, θ. It breaks the condition of the normal THz-wave incidence on the interfaces between media (6). It also increases the optical path, traveled by the THz pulse in the reference window; thus, we observe an effective change of the reference window thickness in (7). For small angular deviations, $\theta < 5°$, the reflectivity change is negligible, and it cannot significantly affect the inverse problem solution [23], [28], [31]. However, changes of the THz-wave optical path can impact the material parameter reconstruction.

We assume this factor by changing the reference window thickness in (11) and (7)

$$l' = l + \Delta l, \quad \Delta l = l\left(\frac{1}{cos(\theta)} - 1\right) \tag{17}$$

where Δl stands for the thickness increment. The inverse problem is solved based on the distorted waveforms, and we compare the reconstructed curves, $n_{\rm rec}$ and $\alpha_{\rm rec}$, with the initial ones, n and α. The results of calculations are presented in Fig. 7. Fig. 7(a) illustrates the typical noise originating from $\theta = 4.4°$ ($\Delta l = 3$ μm). The noise in $n_{\rm rec}$ and $\alpha_{\rm rec}$ have an oscillating character, with the inhomogeneous magnitude. Fig. 7(b) and 7(c) shows the normalized spectral densities of the noise magnitudes, $\Delta n/n$ and $\Delta\alpha/\alpha$, calculated for various Δl (16).

The $\Delta n/n$ and $\Delta\alpha/\alpha$ functions have a symmetric character with respect to the ideal angular orientation of the reference window, $\Delta l = 0$ ($\theta = 0$). The error increases significantly if

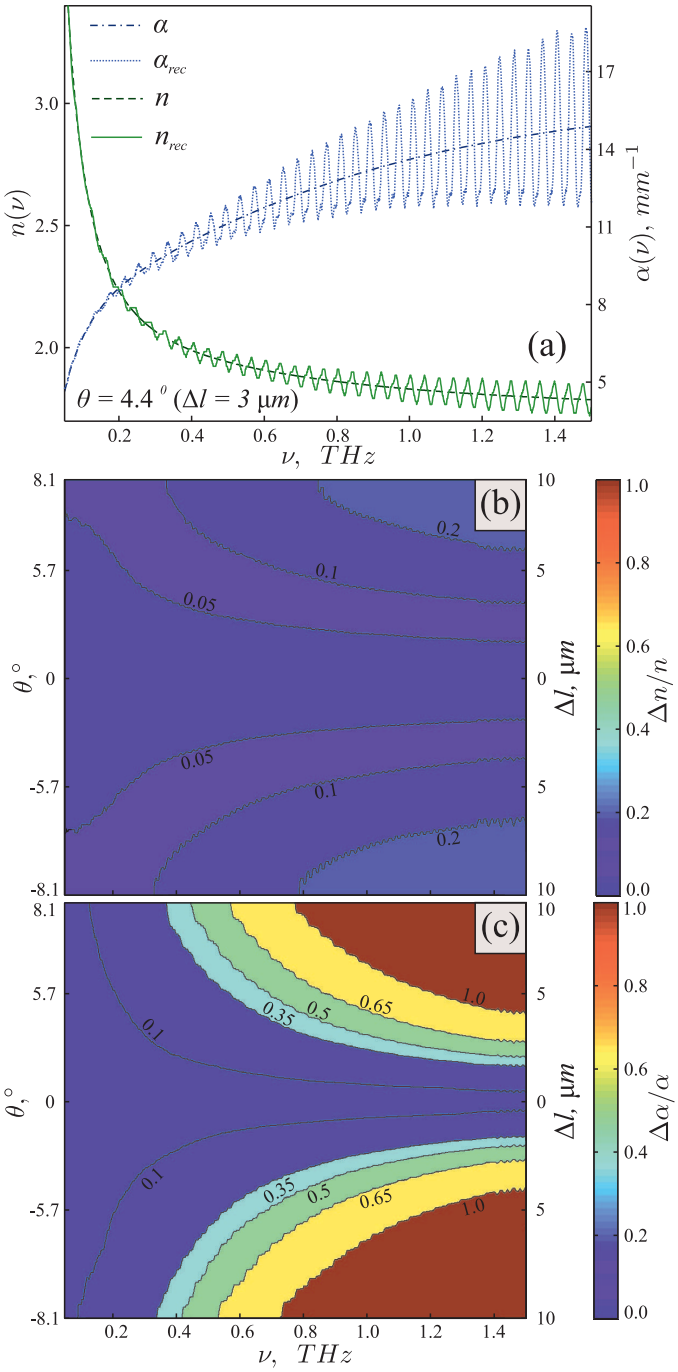

Fig. 7. Impact of the reference window angular deviations (17) on reconstruction of the THz refractive index and absorption coefficient of the skin *in vivo*. (a) Initial model of the THz refractive index and the absorption coefficient, n and α, and the reconstructed curves, $n_{\rm rec}$ and $\alpha_{\rm rec}$, calculated for $\theta = 4.4°$ ($\Delta l = 3$ μm). (b) Normalized spectral density of the refractive index reconstruction error $\Delta n/n$ (16). (c) Normalized spectral density of the absorption coefficient reconstruction error $\Delta\alpha/\alpha$ (16).

$\theta > 2.5°$ ($\Delta l > 1$ μm). Thus, we should satisfy the condition $\theta < 2.5°$ during TPS waveform detection. The specified accuracy of the reference window orientation can be easily achieved by rigidly fixing the window, and so the latter factor does not impact the inverse problem solution.

Besides the considered sources of measurement errors, which are inherent specifically to the described reconstruction technique, there are many other ones exist, for instance, jitters in the TPS delay stage [73] and instabilities of the femtosecond laser [28]. Obviously, these errors are inherent to all the TPS techniques, and they can cause instabilities of the TPS inverse problem solutions. However, systematic studying of all the TPS instabilities is out of scope of the present paper.

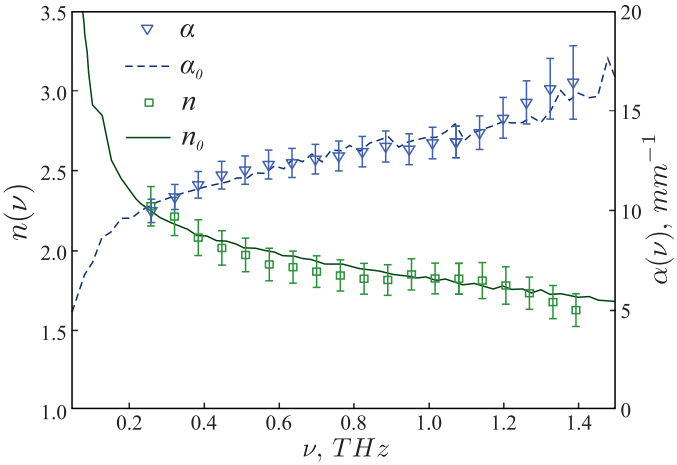

Fig. 8. Comparison of our results on *in vivo* THz spectroscopy of the skin from the arm, n and α, with the well-known data, n_0 and α_0, from [74].

D. Verification of the Method

Before experimental implementation of the proposed method, we have studied the THz materials parameters of the reference THz window (Fig. 1). We have characterized the SiO_2-window using the TPS transmission-mode measurements [28]. Observed THz material parameters agree with the well-known data from [67], and we use them to process the data of *in vivo* measurements of the skin.

To verify the described approach for reconstruction of the THz refractive index and absorption coefficient, we implement it to study *in vivo* the skin from the arm. Fig. 8 shows that the results of our measurements, n and α, agree well with the data from [74], n_0 and α_0.

The error bars in Fig. 8 are calculated using the same approach, which was implemented for studying the stability of the inverse problem solution (Fig. 4). First, we ensured that during the experiment and TPS data processing we have satisfied all the demands associated with the reference window position (see Section III-C). Second, we considered the reconstructed material parameters as an initial condition to solve the direct problem [see (10)–(12)] and to obtain the waveform models. White Gaussian noise, which is inherent to the experimental waveforms, was added to the models of the TPS waveforms, the TPS inverse problem was solved (2), and the error bars were calculated via (14). The described approach to calculate the error bars provides a unique opportunity to estimate the errors of reconstruction considering all the aspects of the reflection mode measurement. Moreover, the described technique can be generalized to study the stability and to analyze the measurement errors for other types of TPS systems [8]–[20].

The reconstruction error varies inhomogeneously with frequency for both THz refractive index and absorption coefficient in the Fig. 8. This feature of the error bars originates both from the spectral inhomogeneities of TPS sensitivity and from the multiple THz-wave reflections in the reference THz window.

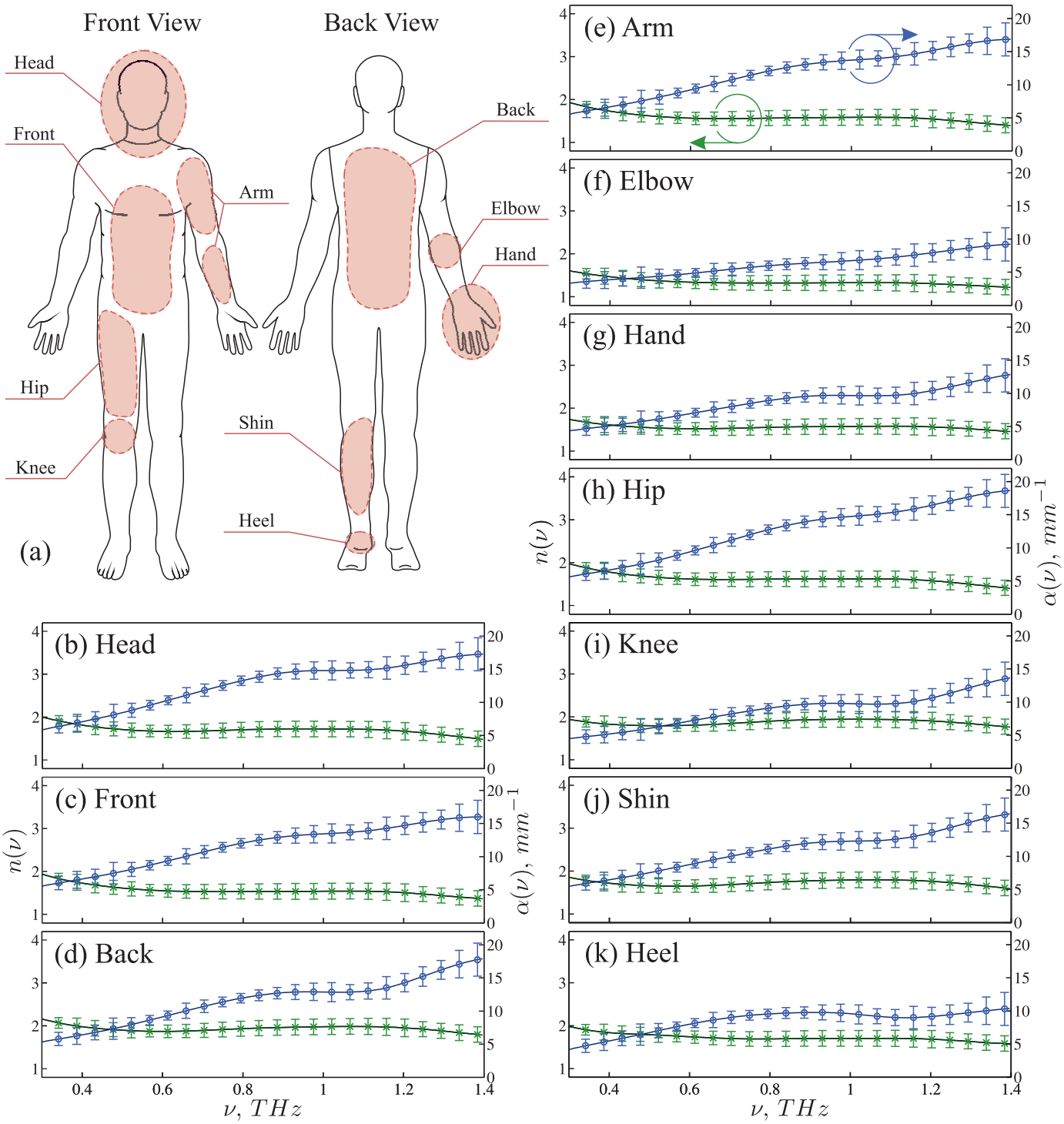

Fig. 9. Variation of the THz refractive index and absorption coefficient of the skin *in vivo* along the human body. Panel (a) schematically represents the human body and considered regions. The curves from (b) to (k) represent the THz characteristics of the skin from the head, the front side of the body, the back side of the body, the arm, the elbow, the hand, the hip, the knee, the shin, and the heel, respectively. The material parameters of the skin are collected from three persons. At least 5 spectral characteristics from each of the listed regions of the body from each of the persons (at least 15 spectral characteristics from each region of interest) were used to calculate the averaged curves n and α.

The error rises dramatically at low (ν<0.2THz) and high (ν>1.4THz) frequencies due to the number of TPS instabilities [28], [73]. Moreover, THz-wave scattering on the surface and in the volume of the tissue sample prevents accurate reconstruction at higher frequencies [60]. Thereby, we do not show the reconstruction results in these frequency ranges.

IV. Measuring the Variation of Refractive Index and Absorbtion Coefficient of the Skin Along the Human Body

We used the proposed algorithm to study *in vivo* the THz refractive index and absorption coefficient of the skin from three

persons. We considered the variation of the THz characteristics of the skin along the body by measuring a number of points from each part of the body from each person, and we systematically analyzed the observed results.

Fig. 9 shows the results of skin spectroscopy. We have grouped the results according to the fluctuations of the THz characteristics along the body. Similar THz refractive index and absorption coefficient are inherent to certain regions of the body, which are marked in Fig. 9(a) with the dashed red lines. Each group represents the results of averaging of at least 5 measurements from each of the three persons (i.e., each group is formed on the basis of at least 15 spectral characteristics). The groups represent the THz refractive index and the absorption coefficient from the head, including the face, the chin, and the neck [Fig. 9(b)]; the front side of the body [Fig. 9(c)]; the back side of the body [Fig. 9(d)]; the arm [Fig. 9(e)]; the elbow [Fig. 9(f)]; the hand [Fig. 9(g)]; the hip [Fig. 9(h)]; the knee [Fig. 9(i)]; the shin [Fig. 9(j)]; and the heel [Fig. 9(k)].

Despite the fact that all the refractive index curves, n, decrease monotonically with frequency and, inversely, all the absorption coefficient curves, α, increase monotonically (Fig. 9), the THz characteristics of the skin varies considerably along the body. The highest THz-wave absorption corresponds to the skin from the head and the hip, and the lowest one corresponds to the skin from the elbow, the knee, and the heel. Since the THz waves penetrate only the epidermis of the skin, the THz characteristics depends exactly on the physical and chemical properties of the epidermis tissue, i.e., on picosecond dynamics in media [29], [74], [75]. The water content in tissue significantly impacts its THz characteristics owing to the high polarity of the water molecule [76], [77]. Obviously, the structure of the epidermis, namely, the thickness of the stratum corneum [33] and the features of the THz-wave scattering on the surface and in the volume of the tissue, affects its characterization in the THz frequency range.

The results of the present paper are of principal importance for further development of novel methods of skin diagnosis and therapy based on THz technology and, in particular, on TPS. All the methods to noninvasively diagnose skin cancers [37]–[40], [60], [61] and burns [56]–[59] based on THz absorption spectroscopy, as well as all the approaches for principal component analysis [40], [60], should be adjusted to account for the variations of the THz refractive index and absorption coefficient along the human body.

V. Conclusion

In conclusion, in this paper we have proposed a method for reconstruction of the THz refractive index and absorption coefficient of *in vivo* tissue using TPS. The method utilizes the reference SiO_2-window to fix the sample during measurements. It accounts satellite THz pulses in TPS waveforms, originating from the multiple THz-wave reflections in the reference window, to accurately solve the inverse problem. We have studied the stability of the inverse problem solution in the presence of various negative factors, and we have verified the proposed method. We have implemented the method to characterize human skin *in vivo*. The observed results agree with the well-known data in general, except for several regions of the skin. Thus, for the elbow, the hand, the knee, and the heel the THz refractive index and absorption coefficient differ from the average values. This result is of principle importance for further development of novel approaches to noninvasively diagnose cancers and burns of the skin using the THz absorption spectroscopy.

References

[1] D. D. Arnone *et al.*, "Applications of terahertz (THz) technology to medical imaging," *Proc. SPIE*, vol. 3828, pp. 209–219, Sep. 1999.

[2] E. Pickwell and V. P. Wallace, "Biomed. applications of terahertz technology," *J. Phys. D: Appl. Phys.*, vol. 39, no. 17, pp. R301–R310, Sep. 2006.

[3] K. Ajito and Y. Ueno, "THz chemical imaging for biological applications," *IEEE Trans. THz Sci. Technol.*, vol. 1, no. 1, pp. 293–300, Sep. 2011.

[4] E. MacPherson, G. P. Gallerano, G.-S. Park, H. Hintzsche, and G. J. Wilmink, "Guest editorial: Terahertz imaging and spectroscopy for biology and biomedicine," *IEEE Trans. THz Sci. Technol.*, vol. 3, no. 4, pp. 354–356, Jul. 2013.

[5] S. Fan, Y. He, B. S. Ung, and E. Pickwell-MacPherson, "The growth of biomedical terahertz research," *J. Phys. D: Appl. Phys.*, vol. 47, no. 37, Sep. 2014, Art. no 374009.

[6] D. H. Auston, "Picosecond optoelectronic switching and gating in silicon," *Appl. Phys. Lett.*, vol. 26, no. 3, pp. 101–103, Feb. 1975.

[7] D. H. Auston and P. R. Smith, "Generation and detection of millimeter waves by picosecond photoconductivity," *Appl. Phys. Lett.*, vol. 43, no. 7, pp. 631–633, Oct. 1983.

[8] D. H. Auston, K. P. Cheung, and P. R. Smith, "Picosecond photoconducting hertzian dipoles," *Appl. Phys. Lett.*, vol. 45, no. 3, pp. 284–286, Aug. 1984.

[9] F. E. Doany, D. Grischkowsky, and C.-C. Chi, "Carrier lifetime versus ion-implantation dose in silicon on sapphire," *Appl. Phys. Lett.*, vol. 50, no. 8, pp. 460–462, Feb. 1987.

[10] K. A. McIntosh, K. B. Nichols, S. Verghese, and E. R. Brown, "Investigation of ultrashort photocarrier relaxation times in low-temperature-grown GaAs," *Appl. Phys. Lett.*, vol. 70, no. 3, pp. 354–356, Jan. 1997.

[11] G. Klatt *et al.*, "Terahertz emission from lateral photo-dember currents," *Opt. Express*, vol. 18, no. 5, pp. 4939–4947, Mar. 2010.

[12] J.-S. Hwang *et al.*, "The dependence of terahertz radiation on the built-in electric field in semiconductor microstructures," *Opt. Express*, vol. 15, no. 8, pp. 5120–5125, Apr. 2007.

[13] L. Xu, X.-C. Zhang, and D. H. Auston, "Terahertz beam generation by femtosecond optical pulses in electro-optic materials," *Appl. Phys. Lett.*, vol. 61, no. 15, pp. 1784–1786, Oct. 1992.

[14] C. Winnewisser, P. U. Jepsen, M. Schall, V. Schyja, and H. Helm, "Electro-optic detection of THz radiation in litao3, linbo3 and ZnTe," *Appl. Phys. Lett.*, vol. 70, no. 23, pp. 3069–3071, Jun. 1997.

[15] G. Gallot and D. Grischkowsky, "Electro-optic detection of terahertz radiation," *J. Opt. Soc. Amer. B*, vol. 16, no. 8, pp. 1204–1212, Aug. 1999.

[16] T. Yasui, S. Yokoyama, H. Inaba, K. Minoshima, T. Nagatsuma, and T. Araki, "Terahertz frequency metrology based on frequency comb," *IEEE J. Select. Topics Quantum Electron.*, vol. 17, no. 1, pp. 191–201, Jan./Feb. 2011.

[17] X. Lu and X.-C. Zhang, "Generation of elliptically polarized terahertz waves from laser-induced plasma with double helix electrodes," *Physical Rev. Lett.*, vol. 108, no. 12, Mar. 2012, Art no 123903.

[18] A. V. Borodin *et al.*, "Transformation of terahertz spectra emitted from dual-frequency femtosecond pulse interaction in gases," *Opt. Lett.*, vol. 38, no. 11, pp. 1906–1908, Jun. 2013.

[19] Y.-D. Hsieh *et al.*, "Terahertz comb spectroscopy traceable to microwave frequency standard," *IEEE Trans. THz Sci. Technol.*, vol. 3, no. 3, pp. 322–330, May 2013.

[20] A. V. Borodin, M. N. Esaulkov, A. A. Frolov, A. P. Shkurinov, and V. Y. Panchenko, "Possibility of direct estimation of terahertz pulse electric field," *Opt. Lett.*, vol. 39, no. 14, pp. 4092–4095, Jul. 2014.

[21] L. Duvillaret, F. Garet, and J.-L. Coutaz, "Highly precise determination of optical constants and sample thickness in terahertz time-domain spectroscopy," *Appl. Opt.*, vol. 38, no. 2, pp. 409–415, Jan. 1999.

[22] T. D. Dorney, R. G. Baraniuk, and D. M. Mittleman, "Material parameter estimation with terahertz time-domain spectroscopy," *J. Opt. Soc. Amer. A*, vol. 18, no. 7, pp. 1562–1571, Jul. 2001.

[23] I. Pupeza, R. Wilk, and M. Koch, "Highly accurate optical material parameter determination with THz time-domain spectroscopy," *Opt. Express*, vol. 15, no. 7, pp. 4335–4350, Apr. 2007.

[24] S. Huang *et al.*, "Improved sample characterization in terahertz reflection imaging and spectroscopy," *Opt. Express*, vol. 17, no. 5, pp. 3848–3854, Mar. 2009.

[25] M. Scheller, "Real-time terahertz material characterization by numerical three-dimensional optimization," *Opt. Express*, vol. 19, no. 11, pp. 10647–10655, May 2011.

[26] G. P. Kniffin and L. M. Zurk, "Model-based material parameter estimation for terahertz reflection spectroscopy," *IEEE Trans. THz Sci. Technol.*, vol. 2, no. 2, pp. 231–241, Mar. 2012.

[27] J. A. Hejase, E. J. Rothwell, and P. Chahal, "A multiple angle method for THz time-domain material characterization," *IEEE Trans. THz Sci. Technol.*, vol. 3, no. 5, pp. 656–665, Sep. 2013.

[28] K. I. Zaytsev *et al.*, "Accuracy of sample material parameters reconstruction using terahertz pulsed spectroscopy," *J. Appl. Phys.*, vol. 115, no. 19, p. 193105, May 2014.

[29] S. O. Yurchenko and K. I. Zaytsev, "Spectroscopy of nafion in terahertz frequency range," *J. Appl. Phys.*, vol. 116, no. 11, p. 113508, Sep. 2014.

[30] D. Stanze, B. Globisch, R. J. B. Dietz, H. Roehle, T. Gobel, and M. Schell, "Multilayer thickness determination using continuous wave THz spectroscopy," *IEEE Trans. THz Sci. Technol.*, vol. 4, no. 6, pp. 696–701, Nov. 2014.

[31] K. I. Zaytsev, A. A. Gavdush, S. P. Lebedev, V. E. Karasik, and S. O. Yurchenko, "A method of studying spectral optical characteristics of a homogeneous medium by means of terahertz time-domain spectroscopy," *Opt. Spectrosc.*, vol. 118, no. 4, pp. 552–562, Mar. 2015.

[32] D. M. Mittleman, S. Hunsche, L. Boivin, and M. C. Nuss, "T-ray tomography," *Opt. Lett.*, vol. 22, no. 12, pp. 904–906, Jun. 1997.

[33] Y. Chen, S. Huang, and E. Pickwell-MacPherson, "Frequency-wavelet domain deconvolution for terahertz reflection imaging and spectroscopy," *Opt. Express*, vol. 18, no. 2, pp. 1177–1190, Jan. 2010.

[34] K. W. Kim, H. Kim, J. Park, J. K. Han, and J.-H. Son, "Terahertz tomographic imaging of transdermal drug delivery," *IEEE Trans. THz Sci. Technol.*, vol. 2, no. 1, pp. 99–106, Jan. 2012.

[35] K. I. Zaytsev, V. E. Karasik, I. N. Fokina, and V. I. Alekhnovich, "Invariant embedding technique for medium permittivity profile reconstruction using terahertz time-domain spectroscopy," *Opt. Eng.*, vol. 52, no. 6, p. 068203, Jun. 2013.

[36] Y. C. Sim, J. Y. Park, K.-M. Ahn, C. Park, and J.-H. Son, "Terahertz imaging of excised oral cancer at frozen temperature," *Biomed. Opt. Express*, vol. 4, no. 8, pp. 1413–1421, Aug. 2013.

[37] R. M. Woodward, V. P. Wallace, D. D. Arnone, E. H. Linfield, and M. Pepper, "Terahertz pulsed imaging of skin cancer in the time and frequency domain," *J. Biol. Phys.*, vol. 29, no. 2–3, pp. 257–259, Jun. 2003.

[38] R. M. Woodward *et al.*, "Terahertz pulse imaging of EX VIVO basal cell carcinoma," *J. Investigative Dermatol.*, vol. 120, no. 1, pp. 72–78, Aug. 2003.

[39] V. P. Wallace *et al.*, "Terahertz pulsed imaging of basal cell carcinoma *ex vivo* and *in vivo*," *Brit. J. Dermatol.*, vol. 151, no. 2, pp. 424–432, Aug. 2004.

[40] S. Nakajima, H. Hoshina, M. Yamashita, C. Otani, and N. Miyoshi, "Terahertz imaging diagnostics of cancer tissues with a chemometrics technique," *Appl. Phys. Lett.*, vol. 90, no. 4, p. 041102, Jan. 2007.

[41] C. B. Reid *et al.*, "Terahertz pulsed imaging of freshly excised human colonic tissues," *Phys. in Medicine and Biology*, vol. 56, no. 14, pp. 4333–4353, Jul. 2011.

[42] P. Doradla, K. Alavi, C. Joseph, and R. Giles, "Detection of colon cancer by continuous-wave terahertz polarization imaging technique," *J. Biomed. Opt.*, vol. 18, no. 9, Sep. 2013, Art no 090504.

[43] L. Rong *et al.*, "Terahertz in-line digital holography of human hepatocellular carcinoma tissue," *Scientific Rep.*, vol. 5, p. 8445, Jan. 2015.

[44] A. J. Fitzgerald *et al.*, "Terahertz pulsed imaging of human breast tumors," *Radiology*, vol. 239, no. 2, pp. 533–540, May 2006.

[45] P. C. Ashworth *et al.*, "Terahertz pulsed spectroscopy of freshly excised human breast cancer," *Opt. Express*, vol. 17, no. 15, pp. 12444–12454, Jul. 2009.

[46] A. J. Fitzgerald, S. Pinder, A. D. Purushotham, P. O'Kelly, P. C. Ashworth, and V. P. Wallace, "Classification of terahertz-pulsed imaging data from excised breast tissue," *J. Biomed. Opt.*, vol. 17, no. 1, p. 016005, Jan. 2012.

[47] A. J. Fitzgerald, E. Pickwell-MacPherson, and V. P. Wallace, "Use of finite difference time domain simulations and Debye theory for modelling the terahertz reflection response of normal and tumour breast tissue," *PLoS ONE*, vol. 9, no. 7, Jul. 2014, Art no E99291.

[48] L. V. Titova *et al.*, "Intense THz pulses cause H2AX phosphorylation and activate DNA damage response in human skin tissue," *Biomed. Opt. Express*, vol. 4, no. 4, pp. 559–568, Apr. 2013.

[49] L. V. Titova *et al.*, "Intense THz pulses down-regulate genes associated with skin cancer and psoriasis: a new therapeutic avenue?," *Scientific Rep.*, vol. 3, p. 2363, Aug. 2013.

[50] D. B. Bennett *et al.*, "Terahertz sensing in corneal tissues," *J. Biomed. Opt.*, vol. 16, no. 5, May 2011, Art no 057003.

[51] D. Crawley, C. Longbottom, V. P. Wallace, B. Cole, D. Arnone, and M. Pepper, "Three-dimensional terahertz pulse imaging of dental tissue," *J. Biomed. Opt.*, vol. 8, no. 2, pp. 303–307, Apr. 2003.

[52] E. Pickwell *et al.*, "A comparison of terahertz pulsed imaging with transmission microradiography for depth measurement of enamel demineralisation in vitro," *Caries Res.*, vol. 41, no. 1, pp. 49–55, Dec. 2007.

[53] C. B. Reid, G. Reese, A. P. Gibson, and V. P. Wallace, "Terahertz time-domain spectroscopy of human blood," *IEEE J. Biomed. Health Informat.*, vol. 17, no. 4, pp. 774–778, Apr. 2013.

[54] K. Jeong *et al.*, "Characterization of blood using terahertz waves," *J. Biomed. Opt.*, vol. 18, no. 10, Oct. 2013, Art no 107008.

[55] C. B. Reid, G. Reese, A. P. Gibson, and V. P. Wallace, "Terahertz time-domain spectroscopy of human blood," *IEEE Trans. THz Sci. Technol.*, vol. 3, no. 4, pp. 363–367, Jul. 2013.

[56] Z. D. Taylor *et al.*, "Reflective terahertz imaging of porcine skin burns," *Opt. Lett.*, vol. 33, no. 11, pp. 1258–1260, Jun. 2008.

[57] M. H. Arbab, T. C. Dickey, D. P. Winebrenner, A. Chen, M. B. Klein, and P. D. Mourad, "Terahertz reflectometry of burn wounds in a rat model," *Biomed. Opt. Express*, vol. 2, no. 8, pp. 2339–2347, Aug. 2011.

[58] P. Tewari *et al.*, "*In vivo* terahertz imaging of rat skin burns," *J. Biomed. Opt.*, vol. 17, no. 4, p. 040503, Apr. 2012.

[59] W. E. Baughman, H. Yokus, S. Balci, D. S. Wilbert, P. Kung, and S. M. Kim, "Observation of hydrofluoric acid burns on osseous tissues by means of terahertz spectroscopic imaging," *IEEE Trans. THz Sci. Technol.*, vol. 3, no. 4, pp. 387–394, Jul. 2013.

[60] K. I. Zaytsev, K. G. Kudrin, V. E. Karasik, I. V. Reshetov, and S. O. Yurchenko, "In vivo terahertz spectroscopy of pigmentary skin nevi: Pilot study of non-invasive early diagnosis of dysplasia," *Appl. Phys. Lett.*, vol. 106, no. 5, Feb. 2015, Art no 053702.

[61] K. I. Zaytsev *et al.*, "In vivo spectroscopy of healthy skin and pathology in terahertz frequency range," in *J. Phys.: Conf. Series*, Jan. 2015, vol. 584, no. 1, p. 012023.

[62] R. L. Barnhill, J. A. Fine, G. C. Roush, and M. Berwick, "Predicting five-year outcome for patients with cutaneous melanoma in a population-based study," *Cancer*, vol. 78, no. 3, pp. 427–432, Jan. 1996.

[63] M. Arumi-Uria, N. S. McNutt, and B. Finnerty, "Grading of atypia in nevi: Correlation with melanoma risk," *Modern Pathol.*, vol. 16, no. 8, pp. 764–771, Aug. 2003.

[64] K. I. Zaytsev, K. P. Tsapenko, P. A. Nosov, and S. O. Yurchenko, "An impact of multiple wave reflections in a flat sample on material parameter reconstruction using THz pulsed spectroscopy," in *J. Phys.: Conf. Series*, Jan. 2005, vol. 584, no. 1, Art no 012005.

[65] M. Kruger, S. Funkner, E. Bründermann, and M. Havenith, "Uncertainty and ambiguity in terahertz parameter extraction and data analysis," *J. Infrared, Millim., THz Waves*, vol. 32, no. 5, pp. 699–715, May 2011.

[66] E. Pickwell, B. E. Cole, A. J. Fitzgerald, V. P. Wallace, and M. Pepper, "Simulation of terahertz pulse propagation in biological systems," *Appl. Phys. Lett.*, vol. 84, no. 12, pp. 2190–2192, Mar. 2004.

[67] D. Grischkowsky, S. Keiding, M. van Exter, and C. Fattinger, "Far-infrared time-domain spectroscopy with terahertz beams of dielectrics and semiconductors," *J. Opt. Soc. Amer. B*, vol. 7, no. 10, pp. 2006–2015, Oct. 1990.

[68] M. Naftaly and R. Dudley, "Methodologies for determining the dynamic ranges and signal-to-noise ratios of terahertz time-domain spectrometers," *Opt. Lett.*, vol. 34, no. 8, pp. 1213–1215, Apr. 2009.

[69] K. I. Zaytsev *et al.*, "An approach for automatic construction of the wavelet-domain de-noising procedure for THz pulsed spectroscopy signal processing," in *J. Phys.: Conf. Series*, Mar. 2014, vol. 486, no. 1, Art no. 012034.

[70] N. V. Chernomyrdin *et al.*, "Wavelet-domain de-noising technique for THz pulsed spectroscopy," *Proc. SPIE*, vol. 9216, Sep. 2014, Art no 921611.

[71] K. I. Zaytsev *et al.*, "Wavelet-domain de-noising of optical coherent tomography data for biomedical applications," in *J. Phys.: Conf. Series*, Jan. 2015, vol. 584, no. 1, Art no. 012013.

[72] R. C. Gonzalez and R. E. Woods, *Digital Image Processing*, 3rd ed. Upper Saddle River, NJ, USA: Prentice Hall, 2007.

[73] N. Vieweg *et al.*, "Terahertz-time domain spectrometer with 90 dB peak dynamic range," *J. Infrared, Millim., THz Waves*, vol. 35, no. 10, pp. 823–832, Oct. 2014.

[74] E. Pickwell, B. E. Cole, A. J. Fitzgerald, M. Pepper, and V. P. Wallace, "*In vivo* study of human skin using pulsed terahertz radiation," *Phys. Medicine Biol.*, vol. 49, no. 9, p. 1595, May 2004.
[75] J.-Y. Chen, J. R. Knab, S. Ye, Y. He, and A. G. Markelz, "Terahertz dielectric assay of solution phase protein binding," *Appl. Phys. Lett.*, vol. 90, no. 24, p. 243901, Jun. 2007.
[76] L. Thrane, R. H. Jacobsen, P. Uhd Jepsen, and S. R. Kieding, "THz reflection spectroscopy of liquid water," *Chemical Phys. Lett.*, vol. 240, no. 4, pp. 330–333, Jun. 1995.
[77] E. S. Zhukova *et al.*, "Vibrational states of a water molecule in a nanocavity of beryl crystal lattice," *J. Chemical Phys.*, vol. 140, no. 22, p. 224317, Jun. 2014.

Kirill I. Zaytsev was born in 1989. He is currently working toward the Ph.D. degree from Bauman Moscow State Technical University (BMSTU), Moscow, Russia.

He is also an associate researcher of Terahertz Technology Laboratory (URL: http://teratech.ru/) at Research and Educational Center "Photonics and Infrared Technology" at BMSTU. His research interests include THz technology, THz pulsed spectroscopy, inverse ill-posed problems in optics, and photonic crystals.

Arseniy A. Gavdush is currently working toward the master's degree from Bauman Moscow State Technical University, Moscow, Russia.

He is also an engineer with Terahertz Technology Laboratory (URL: http://teratech.ru/) at the Research and Educational Center "Photonics and Infrared Technology" at BMSTU. His research interests include THz pulsed spectroscopy, inverse problems in optics, and digital signal processing.

Nikita V. Chernomyrding is currently working toward the master's degree from Bauman Moscow State Technical University, Moscow, Russia.

He is also an engineer with Terahertz Technology Laboratory (URL: http://teratech.ru/) at the Research and Educational Center "Photonics and Infrared Technology" at BMSTU. His research interests include THz pulsed spectroscopy, biomedical applications of THz technology, and digital signal processing.

Stanislav O. Yurchenko was born in 1985. He received the Ph.D. degree in physical and mathematical sciences from from the Bauman Moscow State Technical University, Moscow, Russia, in 2009.

He is currently an associate Professor at Bauman Moscow State Technical University (BMSTU), Moscow, Russia, and a head of the Terahertz Technology Laboratory (URL: http://teratech.ru/) at Research and Educational Center "Photonics and Infrared Technology" at BMSTU. His research interests include condensed matter physics, physics of phase transitions, photonics.